Numerical renormalization-group study of low-lying eigenstates of the antiferromagnetic $S = 1$ Heisenberg chain

Steven R. White
Department of Physics, University of California, Irvine, California 92717

David A. Huse
AT&T Bell Labs, Murray Hill, New Jersey 07974

(Received 3 February 1993; revised manuscript received 23 April 1993)

We present results of a numerical renormalization-group study of the isotropic $S = 1$ Heisenberg chain. The density-matrix renormalization-group techniques used allow us to calculate a variety of properties of the chain with unprecedented accuracy. The ground state energy per site of the infinite chain is found to be $e_0 \cong -1.401\,484\,038\,971(4)$. Open-ended $S = 1$ chains have effective $S = 1/2$ spins on each end, with exponential decay of the local spin moment away from the ends, with decay length $\xi \cong 6.03(1)$. The spin-spin correlation function also decays exponentially, and although the correlation length cannot be measured as accurately as the open-end decay length, it appears that the two lengths are identical. The string correlation function shows long-range order, with $g(\infty) \cong -0.374\,325\,096(2)$. The excitation energy of the first excited state, a state with one magnon with momentum $q = \pi$, is the Haldane gap, which we find to be $\Delta \cong 0.410\,50(2)$. We find many low-lying excited states, including one- and two-magnon states, for several different chain lengths. The magnons have spin $S = 1$, so the two-magnon states are singlets ($S = 0$), triplets ($S = 1$), and quintuplets ($S = 2$). For magnons with momenta near π, the magnon-magnon interaction in the triplet channel is shown to be attractive, while in the singlet and quintuplet channels it is repulsive.

I. INTRODUCTION

Recent improvements in real-space numerical renormalization group (RG) techniques[1–3] have made this method competitive with, and in many ways superior to, other numerical methods, such as quantum Monte Carlo and exact diagonalization, for studies of one-dimensional (1D) quantum systems. The main advance involves the reformulation of the method in terms of density matrices.[2] In the original formulation of the real-space RG method, a block of sites is diagonalized and the lowest-lying eigenstates of the block Hamiltonian are used to construct a new effective Hamiltonian, which one hopes is valid for the low-lying states of the whole lattice. In the density-matrix method we form the new effective Hamiltonian out of the most probable eigenstates of the block density matrix. This change makes the method tremendously more accurate than the original approach. However, finding the density matrix of the block requires one to diagonalize a larger section of the lattice which includes the block, in order to incorporate the effects of the rest of the lattice on the block. Efficient density-matrix algorithms have been developed for finite chains with open or periodic boundary conditions, as well as for an infinite chain, where the chain length steadily increases with each iteration. These methods have been described in detail elsewhere.[3]

In this paper we report results of a density-matrix RG study of the antiferromagnetic $S = 1$ Heisenberg chain, which has been the subject of a large amount of work in the last decade. Besides exhibiting the well-known Haldane gap, this system has been found to have several other fascinating features. For example, the ground state of an open $S = 1$ chain has an effective $S = 1/2$ spin at each end. These effective spins have been observed in real systems containing $S = 1$ chains, such as $Ni(C_2H_8N_2)_2NO_2ClO_4$ (NENP), using magnetic-resonance techniques.[4] The ground state also exhibits a surprising form of topological long-range order, related to a similar type of order found in fractional quantum-Hall-effect systems. There have been a number of theoretical and experimental studies of the spectrum of low-lying excited states of this system.[6–8]

The density-matrix algorithms used here give much more accurate results using open boundary conditions than with periodic boundary conditions. With periodic boundary conditions, each block has two ends which interact with the rest of the lattice, whereas with open boundary conditions, a block has only one active end if it contains either the right or left end of the chain. The effective Hamiltonian of the block must be made from a larger number of states if it must represent two active ends. Thus the results we report here are all for open chains. It is possible, however, to accurately reproduce bulk properties with open chains because we can study very large chains—up to several hundred sites.

A simple understanding of the ground state of the antiferromagnetic Heisenberg spin-1 chain was presented by Affleck, Kennedy, Lieb, and Tasaki (AKLT).[5] Each spin-1 may be viewed as two spin-1/2 spins that combine on site in a fully symmetric triplet wave function. Now let one spin 1/2 on each site pair with one of the spin-1/2 spins on the next site to the left in an antisymmetric singlet wave function, while the other spin-1/2 pairs with a

spin 1/2 on the next site to the right. The unique singlet wave function of the entire chain resulting from this construction captures much of the essential physics of the ground state. (In fact this wave function is the exact ground state of a closely related Hamiltonian with additional biquadratic nearest-neighbor interactions.[5]) With simple free ends, one thus has unpaired spin 1/2's left at each end of the chain. The interaction between these extra half-spins falls off exponentially with the length of the chain, and so in the limit of a long chain one has a four-fold degenerate ground state due to these two free-end spins. Although this and other end effects are quite interesting in their own right and can be captured very accurately using density-matrix algorithms, in this paper we will focus on properties in the bulk of the chain, away from the ends, and so we would like to remove this inconvenient degeneracy.

If one adds a real spin-1/2 spin at each end of the chain, these can each form singlets with half of the last spin 1 in the chain, thereby removing the ground-state degeneracy. Thus for a chain of length L sites our Hamiltonian is

$$H = \sum_{\ell=1}^{L-1} J(\ell)\vec{S}_\ell \cdot \vec{S}_{\ell+1}, \tag{1}$$

where $\vec{S}_1$ and $\vec{S}_L$ are spin-1/2 spins, while all other spins are of spin 1. The couplings are $J(\ell) = 1$ in the bulk of the chain, but may be adjusted at or near the ends of the chain. By varying the couplings at the ends of the chain we may attempt to choose the best boundary conditions for the task at hand. Examples of this are illustrated below. We generally only adjust the final couplings, taking $J(1) = J(L-1) \equiv J_{\rm end}$ and leaving all other couplings at unity.

The total spin commutes with the Hamiltonian (1). We work in an S^z basis in which the good quantum numbers are total S^z and total spin. The couplings will generally be taken to be symmetric, $J(\ell) = J(L-\ell)$, under parity (reversal of the chain), and so parity is an additional good quantum number.

II. GROUND-STATE PROPERTIES

We have examined the ground state of (1) for various boundary conditions. As long as we have the spin-1/2 spins on the ends and only antiferrromagnetic couplings, $J(\ell) > 0$ for all ℓ, the ground state is a singlet (zero total spin). The parity of the ground state is opposite to the parity of the number of sites, L, as is expected from the above AKLT wave function. Most of our results are for even L where the ground state is thus odd under parity.

We are interested in the properties of the translationally invariant infinite chain, and so when we study the ground state we should choose a boundary condition that induces minimal nonuniformity in the ground state away from the ends. To do this we can measure the ground-state expectation value of the local energy,

$$e(\ell) \equiv \langle \vec{S}_\ell \cdot \vec{S}_{\ell+1} \rangle \ , \tag{2}$$

and ask that this be perturbed as little as possible by the boundary condition. Near the end of the chain, $e(\ell)$ does show nonuniformities due to end effects which decay rapidly as one moves away from the end, as illustrated in Fig. 1. When we adjust the end coupling, the minimum end effect is seen at $J_{\rm end} \cong 0.7$ (see Fig. 1).

The ground-state energy can then be obtained by measuring $E(\ell)$ in the center of the chain. However, a significantly more accurate estimate is obtained by measuring energy differences using the infinite-lattice algorithm. In the infinite-lattice method, the size of the lattice grows by 2 at each step. The two additional sites are added in the center of the chain. The total energy of the chain increases in one step by the energy associated with these two sites. Using $J_{\rm end} = 0.7$, the additional energy added in a step divided by two converges very rapidly with increasing L to a very accurate estimate of the ground-state energy per site. The error in the energy due to finite L quickly becomes negligible compared to the truncation error $1 - P(m)$,[3] where m is the number of states kept per block. $P(m)$ is defined as the sum of the first m density-matrix eigenvalues; the corresponding eigenvectors are used in constructing the effective Hamiltonian of a block. Each density-matrix eigenvalue represents the probability of that particular eigenstate, and $1 - P(m)$ thus gives the fractional error involved in representing a block by only m states. Of course, in the course of a calculation the density matrix is diagonalized for a variety of blocks of different sizes; we report the largest value of $1-P(m)$ appearing in the last iteration. (In this case the earlier iterations can be considered merely preliminary to the last iteration.)

Because of the very rapid decrease of $1 - P(m)$ with m, our determination of the ground-state energy is ultimately limited in accuracy by accumulated round-off error in the various parts of the calculation due to the use of 64-bit ("real*8" in FORTRAN) precision. The accuracy of the density-matrix eigenvectors begins to degrade when the associated eigenvalues become less than about

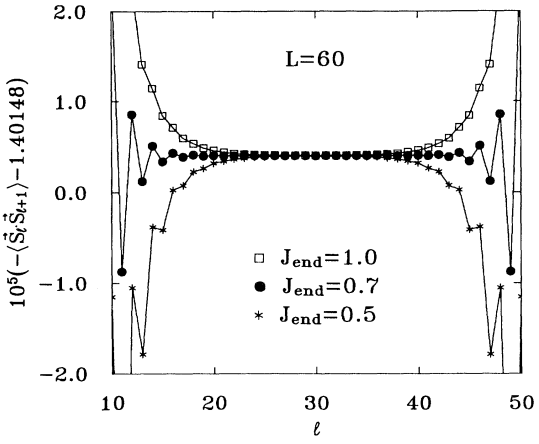

FIG. 1. Local energy in the ground state vs distance along the chain ℓ for a chain of length $L = 60$ and various values of $J_{\rm end}$. The end effect is minimized for $J_{\rm end} \cong 0.7$. Note the highly expanded scale on the vertical axis.

10^{-12}. The primary effect of using these inaccurate eigenvectors is a slight slowdown in the rate of convergence of quantities such as the energy with m. As long as the set of eigenvectors used to represent a block is kept orthonormal to machine precision, which is not difficult, we do not expect any errors associated with including these approximate eigenvectors, only a somewhat slower reduction in the truncation errors. In the case of the ground-state of the $S = 1$ Heisenberg chain, for $m \leq 110$, round-off error is negligible. Table I shows the ground-state energy per spin, e_0, for various values of m, having converged with lattice size in each case. For m ranging from 36 to 86, the error in the energy (determined using the larger-m results) is roughly proportional to $1 - P(m)$, with a coefficient of about 5. Using this slope to correct the results for $m = 110$ gives a corrected estimate of the energy of $e_0 \cong -1.40148403895$. This correction also can be used as an estimate of the uncertainty in the final result; we find (using $m \leq 110$) $e_0 \cong -1.4014840390(2)$. A more accurate result is obtained by correcting the $m = 180$ results in a similar way, yielding $e_0 \cong -1.401484038971(4)$. This last result may be affected by round-off errors larger than the stated error (which is a generous estimate of the truncation error); to estimate the round-off error we would need to run the calculations with higher numerical precision.

The spin-spin correlation function $C(i-j) = \langle S_i^z S_j^z \rangle$ can be measured in a symmetrical fashion on a finite chain by putting i and j equal distances from the center of the chain, and varying their separation. This calculation can be carried out with either the finite-lattice or infinite-lattice method. The correlation function is expected to behave for large l as

$$C(\ell) \approx A(-1)^\ell K_0(\ell/\xi) \approx A(-1)^\ell (\pi\xi/2\ell)^{1/2} e^{-\ell/\xi}, \quad (3)$$

where A is a constant, K_0 is the modified Bessel function, ξ is the correlation length, and the second form holds for $\ell >> \xi$. Figure 2 shows $C(\ell)$ from an infinite-lattice calculation with $m = 180$. The correlation function cannot be measured as accurately as the energy, with the errors as large as 10^{-6} for $\ell \approx 30$. Nevertheless, our results are substantially more accurate than those from quantum Monte Carlo calculations.[9] Unlike the errors in quantum Monte Carlo calculations, the truncation errors from finite m are systematic, rather than random. Figure 3 shows $\xi_\ell \equiv -1/\ln[-C(\ell)/C(\ell-1)]$, which is a measure of a local correlation length, with the true correlation length given by $\xi = \xi_\infty$. For any value of m, the behavior becomes purely exponential for large ℓ, but the limiting correlation length is not especially accurate. The presence of prefactors modifying the simple exponential, as in (3), makes a direct determination of ξ (with no assumptions about prefactors) difficult from this data.

Also shown as the top trace in Fig. 3 is the equivalent decay length for the decay of $\langle S_\ell^z \rangle$ away from the effective $S = 1/2$ spin on an open end of a $S = 1$ chain, i.e., one without a real $S = 1/2$ on the end to remove the degeneracy; here we take the ground state with total

TABLE I. Ground-state energy per site as a function of the number of states kept m. The energy was obtained using the infinite-lattice method, where the lattice size was increased until convergence of all digits shown was obtained. Also shown is the truncation error $1 - P(m)$.

m	e_0	$1 - P(m)$
36	-1.40148379810	5.61×10^{-8}
48	-1.40148401407	4.13×10^{-9}
60	-1.40148403106	1.23×10^{-9}
72	-1.40148403623	3.42×10^{-10}
86	-1.40148403729	1.34×10^{-10}
100	-1.40148403872	2.66×10^{-11}
110	-1.40148403887	1.27×10^{-11}
160	-1.401484038968	4.4×10^{-13}
180	-1.401484038970	1.4×10^{-13}

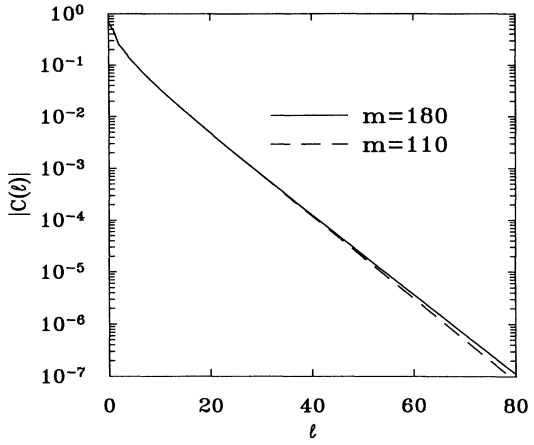

FIG. 2. Spin-spin correlation function $C(\ell)$ as a function of ℓ for two different values of m, the number of states kept per block.

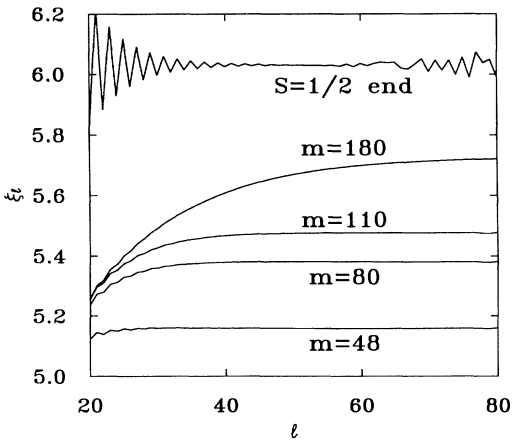

FIG. 3. Local correlation length $\xi_\ell \equiv -1/\ln[-C(\ell)/C(\ell-1)]$ for various m. Also shown is the equivalent decay length for an effective $S = 1/2$ spin at the end of an $S = 1$ chain (with $\langle S_\ell^z \rangle$ replacing $C(\ell)$ in the formula for ξ_ℓ).

$S^z = 1/2$. The decay in this case is expected to be almost purely exponential,[12] in contrast to an earlier report,[11] and our results support this. (The irregular behavior for large ℓ is due to truncation error.) In this case it is easy to determine a decay length of $\xi \cong 6.03(1)$, as was reported earlier.[2] Given that we can measure this decay length accurately, an interesting question is whether this decay length is the same as the correlation length governing the decay of $C(\ell)$. To this end we analyze the data for $C(\ell)$ in a similar manner to Nomura.[10] Figure 4 shows $C(\ell)$ divided by $A(-1)^\ell K_0(\ell/\xi)$, with $\xi = 6.03$ and $A = 0.19934$, for various m. The factor A was determined by requiring the fit to be exact for $\ell = 30$ for the $m = 180$ data. For small ℓ the calculated $C(\ell)$ is very accurate and gives corrections to the assumed form. For intermediate ℓ the data and the assumed form agree extremely well. For large ℓ, the data show systematic deviations, with the value of ℓ for which the deviations appear increasing with m. We conclude that the assumed form works very well for $\ell \geq 15$ and that the decay length and the correlation length are indeed the same, $\xi \cong 6.03$.

It has been conjectured,[13] and limited numerical evidence has supported,[14–19] that a particular type of topological long-range order exists in the spin-1 chain. This order can be measured by the string correlation function

$$g(\ell) = \left\langle S_0^z \left(\prod_{k=1}^{\ell-1} e^{i\pi S_k^z} \right) S_\ell^z \right\rangle. \tag{4}$$

Despite its complicated form, this function is easily measured with the infinite-lattice algorithm. In this algorithm, the left-hand block is built up site by site by adding a site to its right-hand side. (The right-hand block is obtained at each step by reflecting the left-hand block.) The matrix representation of the operator in the brackets of Eq. (4) is built up site by site also. As site k is added to the block, the matrix for the operator $e^{i\pi S_k^z}$ is multiplied onto the right-hand side of $S_0^z(\prod_{l=1}^{k-1} e^{i\pi S_l^z})$, which was formed during earlier steps. The starting point for the buildup of this operator is not the first site of the chain; it is a site far enough from the left end to avoid end effects. At each step of the calculation, we obtain either of two possible measurements of $g(\ell)$: one where we terminate the product at one of the center sites $k+1$ by applying S_{k+1}^z, and one where we couple this string operator with its reflection in the right-hand block to get a measurement of $g(i-j)$ with i and j symmetrically located about the center of the chain. At each step of the iteration, two more sites are added to the center of the chain and the separation $i-j$ grows by 2.

Figure 5 shows the string correlation function $g(\ell)$ as a function of ℓ. The long-range order is clearly evident. The function settles down to its limiting value very rapidly. We have continued the calculation to larger values of ℓ than is shown in the figure; the results stay at the limiting value. For $m = 180$, we find $g(\infty) = -0.374325096(2)$, with convergence to this accuracy starting at $\ell = 50$. For comparison, keeping only $m = 110$ states we find $g(\infty) = -0.374325104$. Exact-diagonalization calculations[14] have estimated $g(\infty) \cong -0.38$ based on a 14-site lattice.

III. ONE-MAGNON EXCITED STATES

Now let us turn to the excited-state spectrum of the antiferromagnetic spin-1 Heisenberg chain. For a uniform chain, momentum is a good quantum number. A sketch of the expected spectrum of low-lying excited states of an infinite chain is shown in Fig. 6. The figure shows only positive momentum; the spectrum is symmetric under momentum reversal (parity). The excitation energy of the lowest-lying excited state is the Haldane gap Δ. This excited state is a triplet with total spin 1 and momentum π in units where the spacing along the chain is $a = 1$. This state is the bottom of the magnon band, whose energy vs momentum is illustrated in Fig. 6. These magnons are the elementary excitations in this system. The rough shape of the magnon dispersion in Fig. 6 is based on the diagonalizations by Parkinson and Bonner[6] and the quantum Monte Carlo results of Takahashi.[7] Below we demonstrate that for momentum near π, the

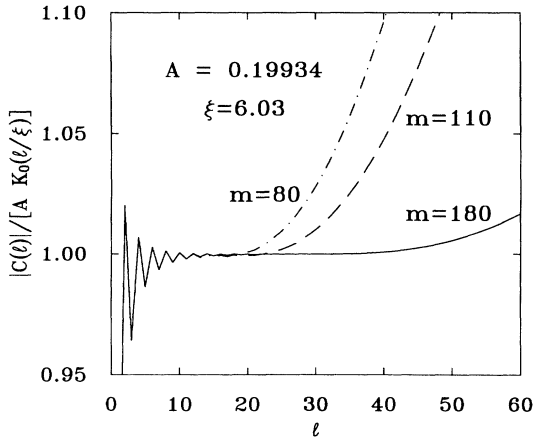

FIG. 4. Ratio of $|C(\ell)|$ to the approximate form $AK_0(\ell/\xi)$ for various values of m, with $A = 0.19934$ and $\xi = 6.03$.

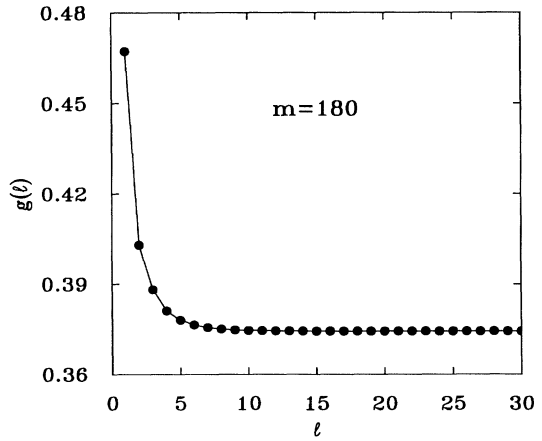

FIG. 5. String correlation function $g(\ell)$.

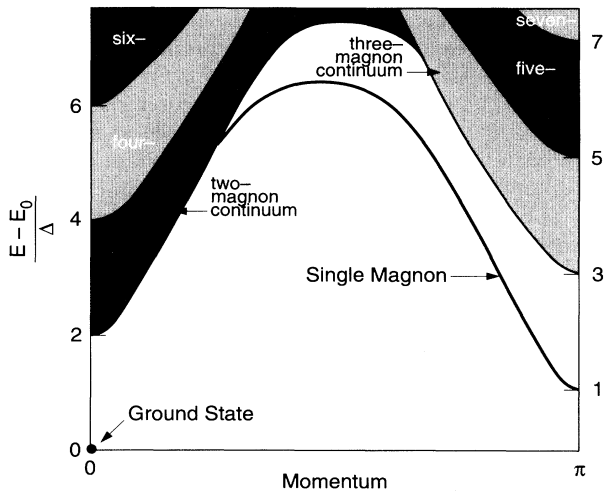

FIG. 6. Schematic of the spectrum of low-lying states for an infinite chain. E is the energy of the excited state, E_0 that of the ground state, and Δ is the Haldane gap. Note that for a given momentum, the one-magnon state, when present, is separated from the continua above it by a gap where there are no excited states.

magnon is indeed a particlelike excitation, and we accurately measure its dispersion relation near π. Inelastic neutron scattering from the qausi-one-dimensional spin-1 antiferromagnet NENP has seen quantitatively the same dispersion, with a splitting of the triplet due to the weak anisotropies in that system.[8]

One may also excite two or more magnons. This results in the multimagnon continua illustrated in Fig. 6. The continua are labeled by the maximum number of magnons that a state of that total excitation energy and total momentum can decay into. Thus, for example, the magnon band disappears into the two-magnon continuum near momentum 0.3π. At this point the single magnon with momentum near 0.3π becomes unstable to decay into two magnons, each with momentum near -0.85π, with the same total energy and the same total momentum modulo 2π. We discuss the two-magnon excited states in some detail below. The multimagnon continua have not yet been detected experimentally.

The wave function of the one-magnon state with momentum q and $S_z = \alpha$ in an infinite chain is expected to be of the form

$$|q,\alpha\rangle = \sum_{\ell} e^{iq\ell} c^{\dagger}_{q,\alpha}(\ell)|0\rangle, \tag{5}$$

where $|0\rangle$ is the ground state. The magnon creation operator $c^{\dagger}_{q,\alpha}(\ell)$ consists of spin operators and products of spin operators in the vicinity of site ℓ. If the magnon were truly a point particle, the creation operator would be simply a spin operator at site ℓ. The true magnon creation operator $c^{\dagger}_{q,\alpha}(\ell)$ also contains products of spin operators away from site ℓ. The weight of these multisite terms presumably decays as one moves away from site ℓ with some characteristic length which is thus a measure of the size of the magnon as a particle. If this particle size is smaller than the length of our finite chain, we expect the magnon to propagate as a free particle in the bulk of the chain, scattering only at the ends of the chain where translational invariance is broken.

For our finite-length chains with spin 1/2's on the ends the lowest-lying few excited states are single-magnon triplet states, with the magnons having particle-in-a-box spatial wave functions. This can be seen by examining the spin density $\langle S^z_i \rangle$ in the $S^z = 1$ states; some examples are illustrated in Fig. 7. We label these single-magnon states by their principal quantum number n. For $J_{\rm end} \geq 0.51$ the principal quantum number counts the number of maxima in the smooth part of $\langle S^z_i \rangle$. The patterns in Fig. 7 are those expected for the probability densities (the square of the modulus of the wave function) for the eigenstates of a particle in a box. Note for Fig. 7 we have adjusted the end coupling to $J_{\rm end} = 1.5$ where the amplitude of the wave function is minimal at the ends to minimize scattering into other states. That the magnons are behaving as particles of finite size carrying energy and spin is seen by noting that the excess energy above the ground state is distributed along the chain with the same pattern as the spin and these patterns are just those expected for particle-in-a-box eigenstates. Although momentum is not a good quantum number in this chain with ends, the nice periodicity of the spin density away from the ends shows that the magnon wave function is, to a good approximation, a sum of two momentum eigenstates with equal and opposite momenta, thus producing a standing wave. The magnitude of the deviation of the momentum from zero or π can thus be deduced from the period of the spin pattern. To distinguish between momenta near zero and momenta near π, one must look at the sign of the wave function, which is not detected by the spin density. For even length chains the parity operation exchanges sublattices, and so a state's eigenvalue under parity can be used to determine whether the momentum is near zero or near π.

The interaction of the magnon with the ends of the

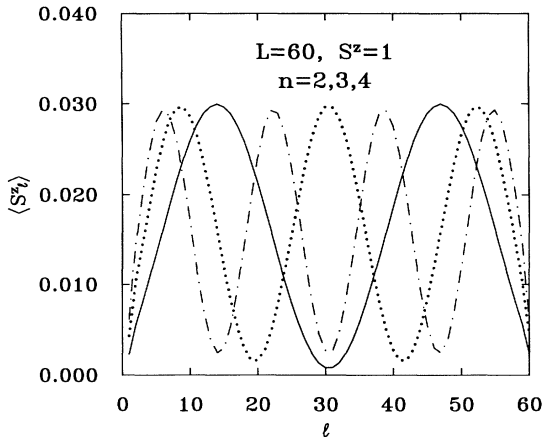

FIG. 7. Local spin densities for the one-magnon excited states with principal quantum numbers $n = 2$, 3, and 4, and total $S^z = 1$, for a chain of length $L = 60$ and $J_{\rm end} = 1.5$.

chain can be adjusted via the coupling at the ends, $J_{\rm end}$. Thus we do not have just a particle in a box with simple hard walls. The potential energy of the magnon is uniform in the bulk of the chain, infinite outside the chain, but may be either negative (attractive) or positive (repulsive) near the chain ends. By adjusting $J_{\rm end}$ we can adjust this potential near the chain ends and thereby the momenta of the magnon eigenstates. In particular, we have found the end coupling, $J_{\rm end} = 0.5088$, which makes the spin and energy densities of the lowest single-magnon state most uniform near the middle of the chain, as shown in Fig. 8. This effectively puts the magnon into the lowest state in the magnon band, with momentum π. The energy of this lowest magnon is the Haldane gap Δ and can be estimated from the ratio of the excess energy density to the spin density near the middle of the chain where end effects are minimal. Results for Δ for various m and L are shown in Table II. From chains with length up to $L = 130$ we estimate $\Delta = 0.41050(2)$. The estimated error comes from the same sort of analysis using $1 - P(m)$ used for the ground-state energy.

At the end of the chain, momentum is not conserved and so single magnons with momenta near π can scatter into virtual two-magnon states with total momenta near zero. These evanescent two-magnon states beat against the one-magnon state, producing the oscillations with spatial period 2 that are seen in Fig. 8. To minimize this end effect and thus get the purest single-magnon particle-in-a-box states we may adjust the end coupling to $J_{\rm end} = 1.5$ where the spin density seems smoothest near the ends, as in Fig. 7. We would like to map out the entire single-magnon band, and hope to find techniques to target high-lying states in that band, but here we only report our results for the readily accessible low-lying states in that band.

To determine these low-lying states, at each step of the calculation we must diagonalize to find several of the lowest-lying states for a particular S^z, not just the lowest state.[3] Each of these states contributes equally in forming the density matrix of a block, which is then diagonalized in the usual way to get the states to be kept. Up to about 20 states can be targeted in this fashion. To facilitate finding singlet states in the channel $S^z = 0$ in the presence of numerous triplet states, we have incorporated spin-inversion symmetry ($S^z \to -S^z$) into the program. For even-length chains we find states with $S = 0, 2, \ldots$ have an eigenvalue $I = -1$ under spin inversion, while states with $S = 1, 3, \ldots$ have $I = 1$. Spin inversion is not a symmetry for $S^z \neq 0$. Thus we can obtain the lowest up to 20 states in each symmetry sector: $S^z = 0$ and $I = -1$, $S^z = 0$ and $I = 1$, $S^z = 1$, $S^z = 2$, etc.

The case we have examined in most detail is $L = 60$ and $J_{\rm end} = 1.5$, where we have accurate results for the lowest eight single-magnon states. (The rest of the excited states obtained are two-magnon states.) For shorter chains we can obtain fewer one-magnon states, but, nev-

TABLE II. Estimated Haldane gap Δ as a function of the number of states kept m and length of chain L. Also shown is the truncation error $1 - P(m)$.

m	L	Δ	$1 - P(m)$
48	120	0.4123234	2.894×10^{-7}
64	120	0.4115262	4.346×10^{-8}
80	120	0.4108767	1.291×10^{-8}
100	120	0.4105433	1.900×10^{-9}
120	100	0.4105079	6.783×10^{-10}
120	120	0.4105073	7.152×10^{-10}
120	130	0.4105072	7.291×10^{-10}
140	120	0.4105020	2.916×10^{-10}

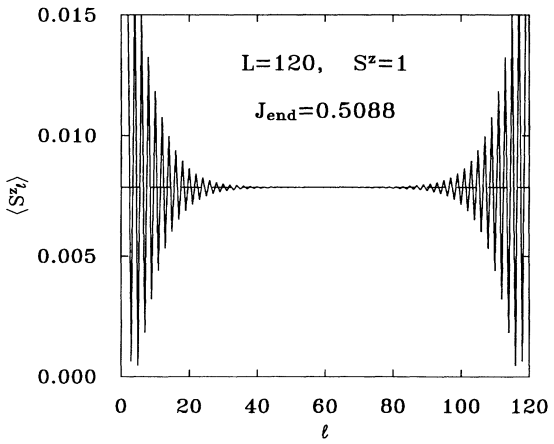

FIG. 8. Local spin density for the lowest-lying one-magnon state with total $S^z = 1$, $L = 120$, and $J_{\rm end} = 0.5088$.

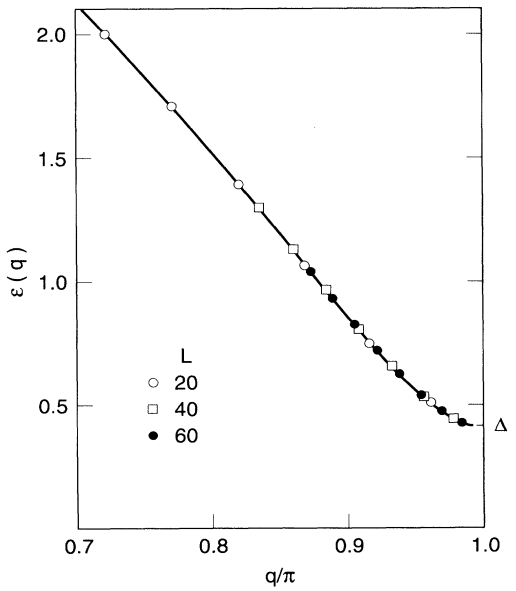

FIG. 9. Single-magnon energies $\epsilon(q)$ from the low-lying one-magnon states for $L = 20, 40$, and 60 with $J_{\rm end} = 1.5$. The absolute value of the momentum q is obtained from the wavelength of these standing-wave eigenstates.

ertheless, these states extend to higher energies: The dispersion obtained from $L = 20, 40$, and 60 with $J_{\text{end}} = 1.5$ is shown in Fig. 9. Note the inflection point in the dispersion, which occurs near momentum 0.85π; this inflection point plays an important role in the two-magnon states, as is discussed below.

The parity of the lowest-lying single-magnon state for these even length chains is even, and thus opposite to that of the ground state. This shows that the smooth-looking densities in Fig. 7 arise from a magnon wave function that indeed does have a momentum near π, thus changing sign between adjacent sites while its amplitude slowly varies. Since the spin density is roughly proportional to the square of the modulus of the local wave function, it does not detect the alternation in sign. The parities alternate with increasing principal quantum number n in the discrete series of single-magnon states for a given L, as expected for a series of particle-in-a-box eigenstates.

IV. TWO-MAGNON STATES AND MAGNON-MAGNON INTERACTIONS

Let us now consider the two-magnon continuum, whose minimum is at energy 2Δ and zero momentum. The first question we must address is, what are the statistics of the magnons? The naive, and correct, expectation is that since they are spin-1 particles, they must be bosons. The local operators that create or annihilate a magnon are, as discussed above, presumably linear combinations of the spin operators in that region and higher-order composites of those spin operators. Since spin operators on different sites commute, we expect that the local magnon operators at two well-separated locations do commute. Thus the statistics should be bosonic and the full wave function symmetric under exchange of two magnons. The magnon operators will not commute when the magnons are close; this reflects the magnon-magnon interactions.

A two-magnon state may have a total spin of $S = 0$, 1, or 2. The spin wave function is antisymmetric under magnon exchange for $S = 1$, and so the spatial wave function must also be antisymmetric to make the full wave function symmetric. For $S = 0$ and $S = 2$ the spin and spatial wave functions are both symmetric. We have been able to access the lowest-lying two-magnon states in each spin channel. We have the fewest two-magnon states (typically five or six) for the triplet ($S = 1$) channel, because the one-magnon states have the same quantum numbers and must be produced at the same time. Each two-magnon state can be identified as the scattering state of two of the elementary one-magnon particle-in-a-box states by using the quantum numbers, parity, and total energy. The energy of interaction is the difference between the sum of the excitation energies of the two one-magnon states and that of the two-magnon state. This identification of the two-magnon states is fairly straightforward because the energies of interaction are mostly smaller than the gaps (due to the finite chain length) between the one-magnon states. We find that the magnons interact attractively in the triplet channel ($S = 1$) and repulsively in the other two spin channels. For the case of $L = 60$ and $J_{\text{end}} = 1.5$, the interaction energies are listed in Table III. Note that when the two magnons are in the same "orbital" they can only make a symmetric spatial wave function, and so there is no such $S = 1$ two-magnon state.

The fact that the magnons attract in the triplet channel and repel in the other channels can be understood as a sort of "Hund's rule" for spin-1 bosons. If there is a strong on-site repulsion between magnons, this will not affect the interaction energy in the triplet channel, where the spatial wave function is antisymmetric and thus has a node when the magnons are on the same site. Such an on-site repulsion will lead to repulsion in the other two channels. If, in addition, there is a weaker attraction when the magnons are on nearby but not identical sites, this will make the net interaction in the triplet channel attractive, while the other two channels remain repulsive.

TABLE III. Energies of one- and two-magnon states for $L = 60$ and $J_{\text{end}} = 1.5$. The first two rows of the table show the absolute value of the momentum and the excitation energy of the lowest five one-magnon states, indexed by their principal quantum numbers n. The remainder of the table shows the energy of interaction for the two-magnon states with total spin S made from magnons with principal quantum numbers n and n'. For example, the lowest-lying two-magnon state is $n = 1$, $n' = 2$, and $S = 1$ with excitation energy $0.4265 + 0.4723 - 0.009 \cong 0.890$. NSS ("no such state") denotes states that do not exist, and NA denotes states that we did not access.

		n				
		1	2	3	4	5
	q/π	0.9851	0.9698	0.9543	0.9385	0.9225
	$\epsilon(q)$	0.4265	0.4723	0.5415	0.6272	0.7239
	$S = 0$	0.052	0.078	0.100	0.116	NA
$n' = 1$	$S = 1$	NSS	-0.009	-0.015	-0.022	NA
	$S = 2$	0.041	0.061	0.075	0.083	0.088
	$S = 0$	0.078	0.081	0.104	NA	NA
$n' = 2$	$S = 1$	-0.009	NSS	-0.020	-0.026	NA
	$S = 2$	0.061	0.059	0.073	0.081	NA
$n' = 3$	$S = 2$	0.075	0.073	0.070	0.078	NA

We have not thought of a reason for why the repulsion is stronger in the singlet ($S = 0$) channel than it is in the quintuplet ($S = 2$) channel.

We have also found some three-magnon states. These can be easily found for total $S^z = 3$, where they are the lowest-lying states. For short enough chains we can also access three-magnon states for smaller S^z. The three-magnon states occur only at energies above 3Δ, as expected. We have not looked at enough three-magnon states to provide a useful characterization of the three-magnon interactions.

One interesting feature of the two-magnon continuum is the formation of a bound state in the triplet channel that occurs near momentum 0.3π and energy 5Δ. We have not been able to directly observe this part of the spectrum because it is too high in energy. The number of states rapidly proliferates once one enters the three-magnon continuum, and so the highest-energy triplet excited states we have been able to access are those near the bottom of the three-magnon continuum, which is well below the energy where the bound state first forms. However, we do know the one-magnon dispersion $\epsilon(q)$ fairly well, and that the magnons attract in the triplet channel, while they repel in the other two channels.

Thus let us take a phenomenological approach to the two-magnon states. The magnons are particlelike excitations above the ground state. Let us view the ground state as the vacuum, the magnons as particles, and assume the interactions are weak. We consider the phenomenological two-magnon Hamiltonian

$$H = \int dq \epsilon(q) c_\alpha^\dagger(q) c_\alpha(q) + \int dQ dq_1 dq_2 c_\alpha^\dagger(q_1) c_\beta^\dagger(Q - q_1) \times V_{\alpha\beta\gamma\delta}(Q, q_1, q_2) c_\gamma(q_2) c_\delta(Q - q_2), \quad (6)$$

where $c_\alpha(q)$ creates a magnon with $S^z = \alpha$ and momentum q, etc., and the repeated subscripts $\alpha, \beta, \ldots$ are summed over -1, 0, and $+1$. This phenomenological Hamiltonian explicitly conserves total momentum Q as it must, and the interaction $V_{\alpha\beta\gamma\delta}$ must be such that it conserves total spin. It also conserves magnon number, which is an approximation. We will use this phenomenology near the bottom of the two-magnon continuum at total momenta less than $\pi/2$; we will also consider the one-magnon state that forms at the high end of this momentum range to be a bound state of two magnons. Thus processes that do not conserve magnon number here involve states in the three- or more-magnon continua, which are well above the bottom of the two-magnon continuum in this regime. We assume the interactions are weak enough that the approximation of neglecting these high-energy magnon nonconserving processes is appropriate.

The single-magnon dispersion relation $\epsilon(q)$ has inflection points near $|q| = 0.85\pi$ that separate regions of upward curvature or positive effective mass, and downward curvative or negative effective mass. The bottom of the two-magnon continuum reflects this in having inflection points near $|Q| = 0.3\pi$. For total momenta below the inflection point the two-magnon state at the bottom of the continuum consists of two magnons with identical momenta $|q| = \pi - |Q|/2$ and positive effective mass. If we go to the "center-of mass" frame, considering only the relative coordinates and momenta of the magnons, our two-magnon problem then becomes a single particle in a potential. For this one-dimensional system, if the potential is at all attractive in the spatially symmetric scattering state, a bound state will form. But we have found that the interaction is repulsive in the symmetric channels, and so we do not expect any bound states there. For finite, positive effective mass, a bound state in the antisymmetric channel will not form for arbitrarily small attraction, but only above a threshold. Thus it is consistent to have an attraction in the triplet channel, but no bound state, as is the case here at low enough $|Q|$.

At the inflection point in the magnon band the fourth derivative of the magnon energy $\epsilon(q)$ with respect to q is positive. This means that at the inflection point in the bottom of the two-magnon continuum, the two-magnon state at the bottom still consists of two magnons with identical momenta. But here once one goes to the "center-of-mass" frame, the single particle now has a k^4 dispersion, where k is the relative momentum. With this dispersion, a bound state must form for arbitrarily small attraction even in the antisymmetric channel. Thus we conclude that the triplet bound state must first form at a total momentum below that of the inflection point in the bottom of the two-magnon continuum. This result is consistent with what is known so far about this part of the spectrum, but it would be interesting to somehow get more accurate information about this regime to develop and test this phenomenological approach more thoroughly.

V. CONCLUSIONS

Using density-matrix numerical renormalization-group techniques, we have calculated a variety of properties of the Heisenberg chain with unprecedented reliability and accuracy. The results we have obtained largely support conclusions obtained from a variety of other methods over the last decade. In the case of the Haldane gap Δ, previous numerical work had established with reasonable certainty the existence of a gap, in agreement with Haldane's conjecture, with $\Delta \cong 0.41$. Our results must remove all remaining doubt, and provide an accurate value for the gap, $\Delta = 0.41050(2)$. We were able to determine the ground-state energy per site of the infinite chain to especially high accuracy, $e_0 \cong -1.401484038971(4)$. The correlation length was found to be identical to the decay length of the local spin moment away from the effective $S = 1/2$ spins on the ends of open $S = 1$ chains, with $\xi \cong 6.03(1)$.

In the case of the string correlation function $g(\ell)$, which measures a form of topological long-range order similar to that found in fractional quantum-Hall-effect systems, previous numerical work had been limited to exact diagonalizations of chains with at most 14 sites. These results suggested that there was long-range topological order, with $g(\infty) \cong -0.38$. We were able to verify the exis-

tence of long-range order beyond any doubt and found $g(\infty) = -0.374325096(2)$.

We were able to determine the properties of a number of the lowest-lying excited states, including one- and two-magnon states, for several different chain lengths, including the determination of the magnon-magnon interactions for magnons with momenta near π. The magnon-magnon interaction in the triplet channel is attractive, while in the singlet and quintuplet channels it is repulsive. Since the numerical techniques used here use a real-space basis, total momentum is not available to use as a quantum number and high-lying one-magnon states with momentum near $\pi/2$ could not be studied. We hope to develop techniques for studying these states in the future.

Note added in proof. We have received a paper from Erik Sorensen and Ian Affleck that shows that the low-lying multimagnon excited states are well approximated by the eigenstates of hard-core bosons. These hard-core boson eigenstates are in turn simply related to those of noninteracting spinless fermions. This introduces a different, and physically more appropriate, way of labeling the multimagnon states than we use above. The classification we have used, i.e., in Table III, is implicitly based on noninteracting bosons as the reference states. For multimagnon wave functions that are fully antisymmetric in space, such as the triplet ($S = 1$) two-magnon states, the eigenstates are identical in the noninteracting and hard-core limits because they vanish whenever two magnons are on the same site. However, for the other states the eigenfunctions in the two limits differ substantially. For example, the singlet ($S = 0$) or quintuplet ($S = 2$) two-magnon eigenstate in the noninteracting limit with orbitals n and n' occupied, with $n' \geq n$, evolves continuously as an on-site repulsion is turned on into the hard-core boson eigenstate which is obtained from the two-fermion eigenstate with orbitals $n_1 = n$ and $n_2 = n' + 1$ occupied. Thus in the labeling scheme of Sorensen and Affleck that derives from this hard-core limit, the lowest-lying two-magnon state in each channel has orbitals $n_1 = 1$ and $n_2 = 2$ occupied. It is clear from the results of Sorensen and Affleck, as well as our results, that the noninteracting limit is actually a rather poor approximation for multimagnon eigenstates that are not spatially fully antisymmetric. Thus we feel that Sorensen and Affleck's method of classifying multimagnon states based on hard-core boson eigenstates should be preferred over the labeling scheme we used in this paper. We thank them for communicating their results prior to publication.

ACKNOWLEDGMENTS

This work was supported by the Office of Naval Research under Grant No. N00014-91-J-1143 (S.R.W.) and in part by the University of California through an allocation of computer time on the UC Irvine Convex. Calculations were also performed at SDSC.

[1] S.R. White and R.M. Noack, Phys. Rev. Lett. **68**, 3487 (1992).
[2] S.R. White, Phys. Rev. Lett. **69**, 2863 (1992).
[3] S.R. White (unpublished).
[4] S. H. Glarum, S. Geschwind, K. M. Lee, M. L. Kaplan, and J. Michel, Phys. Rev. Lett. **67**, 1614 (1991).
[5] I. Affleck, T. Kennedy, E. H. Lieb, and H. Tasaki, Phys. Rev. Lett. **59**, 799 (1987).
[6] J. B. Parkinson and J. C. Bonner, Phys. Rev. B **32**, 4703 (1985).
[7] M. Takahashi, Phys. Rev. Lett. **62**, 2313 (1989).
[8] S. Ma, C. Broholm, D. H. Reich, B. J. Sternlieb, and R. W. Erwin, Phys. Rev. Lett. **69**, 3571 (1992).
[9] S. Liang, Phys. Rev. Lett. **64**, 1597 (1990).
[10] K. Nomura, Phys. Rev. B **40**, 2421 (1989).
[11] M. Hagiwara, K. Katsumata, I. Affleck, B.I. Halperin, and J.P. Renard, Phys. Rev. Lett. **65**, 3181 (1990).
[12] I. Affleck (private communication).
[13] K. Rommelse and M. den Nijs, Phys. Rev. Lett. **59**, 2578 (1987).
[14] S.M. Girvin and D. P. Arovas, Phys. Scr. T **27**, 156 (1989).
[15] Y. Hatsugai, J. Phys. Soc. Jpn. 61, 3856 (1992).
[16] F.C. Alcaraz and Y. Hatsugai, Phys. Rev. B **46**, 13914 (1992).
[17] Y. Hatsugai and M. Kohmoto, Phys. Rev. B **44**, 11789 (1991).
[18] K. Hida, Phys. Rev. B **45**, 2207 (1992).
[19] M. Kohmoto and H. Tasaki, Phys. Rev. B **46**, 3486 (1992).

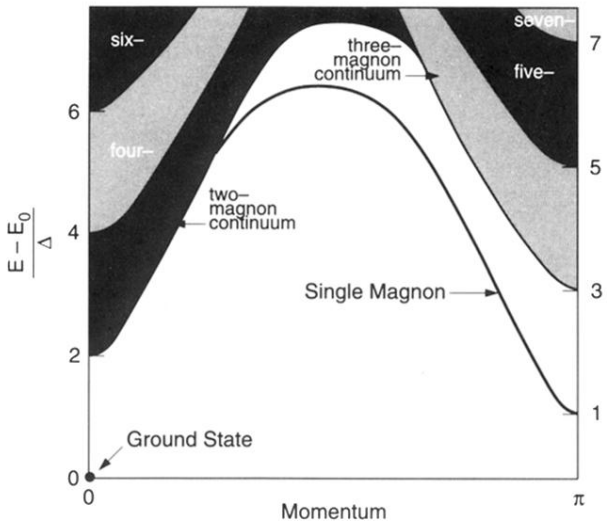

FIG. 6. Schematic of the spectrum of low-lying states for an infinite chain. E is the energy of the excited state, E_0 that of the ground state, and Δ is the Haldane gap. Note that for a given momentum, the one-magnon state, when present, is separated from the continua above it by a gap where there are no excited states.